DMD Fast Forward. Published on March 2, 2017 as DOI: 10.1124/dmd.116.074344
This article has not been copyedited and formatted. The final version may differ from this version.

Effects of MicroRNA-34a on the Pharmacokinetics of Cytochrome P450 Probe Drugs in Mice

Joseph L. Jilek, Ye Tian, and Ai-Ming Yu

Department of Biochemistry & Molecular Medicine, Comprehensive Cancer Center, UC Davis School of Medicine, 2700 Stockton Boulevard, Sacramento, CA 95817, USA (J.L.J., Y.T., A.-M.Y.); Key Laboratory for Space Bioscience and Biotechnology, Institute of Special Environmental Biophysics, School of Life Sciences, Northwestern Polytechnical University, Xi'an, Shaanxi, 710072, China (Y.T.)

DMD Fast Forward. Published on March 2, 2017 as DOI: 10.1124/dmd.116.074344
This article has not been copyedited and formatted. The final version may differ from this version.

Running Title: miR-34a marginally alters CYP probe drug PK

Address correspondence to: Prof. Ai-Ming Yu, Department of Biochemistry & Molecular Medicine, UC Davis School of Medicine, 2700 Stockton Blvd., Room 2132, Sacramento, CA 95817. Tel: +1 916-734-1566; Fax: +1 916-734-4418; Email: aimyu@ucdavis.edu.

Number of text pages: 42

Number of tables: 7

Number of figures: 5

Number of references: 41

Number of words in abstract: 238

Number of words in introduction: 614

Number of words in discussion: 1407

Abbreviations: 3-MC, 3-methylcholanthrene; α-NF, alpha-napthoflavone; APAP, acetaminophen; AUC, area under the plasma drug concentration versus time curve; CLZ, chlorzoxazone; CYP, cytochrome P450; DDI, drug-drug interactions; DXM, dextromethorphan; DXO, dextrophan; DIC, diclofenac; KTZ, ketoconazole; LC-MS/MS, liquid chromatography tandem mass spectrometry; MDZ, midazolam; miR-34a, microRNA-34a; PHE, phenacetin; PCN, pregnenolone-16α-carbonitrile; PK, pharmacokinetics; PXR, pregnane X receptor; 1'-OH-MDZ, 1'-hydroxymidazolam; 4'-OH-DIC, 4'-hydroxydiclofenac; 6-OH-CLZ, 6-hydroxychlorzoxazone.

Abstract

MicroRNAs (miR) including miR-34a have been shown to regulate nuclear receptor, drug-metabolizing enzyme and transporter gene expression in various cell model systems. However, to what degree miRNAs affect pharmacokinetics (PK) at the systemic level remains unknown. Additionally, miR-34a replacement therapy represents a new cancer treatment strategy, although it is unknown if miR-34a therapeutic agents could elicit any drug-drug interactions (DDI). To address this question, we refined a practical single-mouse PK approach and investigated the effects of a bioengineered miR-34a agent on the PK of several Cytochrome P450 (CYP) probe drugs (midazolam, dextromethorphan, phenacetin, diclofenac, and chlorzoxazone) administered as a cocktail. This approach involves manual serial blood microsampling from a single mouse and requires a sensitive LC-MS/MS assay, which was able to illustrate the sharp changes in midazolam PK by ketoconazole and pregnenolone 16α-carbonitrile as well as phenacetin PK by α-napthoflavone and 3-methylcholanthrene. Surprisingly, 3-methylcholanthrene also decreased systemic exposure to midazolam, while both pregnenolone 16α-carbonitrile and 3-methylcholanthrene largely reduced the exposure to dextromethorphan, diclofenac and chlorzoxazone. Finally, the biologic miR-34a agent had no significant effects on the PK of cocktail drugs, but caused a marginal (45-48%) increase in systemic exposure to midazolam, phenacetin, and dextromethorphan in mice. *In vitro* validation of these data suggested that miR-34a slightly attenuated intrinsic clearance of dextromethorphan. These findings from single-mouse PK and corresponding mouse liver microsome models suggest that miR-34a might have minor or no effects on the PK of CYP-metabolized drugs co-administered.

DMD Fast Forward. Published on March 2, 2017 as DOI: 10.1124/dmd.116.074344
This article has not been copyedited and formatted. The final version may differ from this version.

Introduction

MicroRNAs (miRNA or miR) are a family of short, noncoding RNAs (ncRNA) that govern various cellular processes through posttranscriptional regulation of target gene expression (Ambros, 2004). Recent studies have demonstrated that many miRNAs are able to modulate the expression of nuclear receptors, drug-metabolizing enzymes and transporters, and consequently alter cellular drug metabolism and disposition capacities (Yu, 2009; Ingelman-Sundberg et al., 2013; Yokoi and Nakajima, 2013; Yu et al., 2016). As an example, miR-34a was shown to directly regulate hepatocyte nuclear factor 4α (HNF4α or NR2A1) (Takagi et al., 2010), 9-cis retinoic acid receptor alpha (RXRα or NR2B1) (Oda et al., 2014), and nuclear factor (erythroid-derived 2)-like 2 (Nrf2 or NFE2L2) (Huang et al., 2014) in a number of cell line models. In addition, a negative correlation between Cytochrome P450 3A4 (CYP3A4) and miR-34a levels in a set of human liver samples was also identified (Lamba et al., 2014). Nevertheless, it is unknown to what levels miRNAs may affect pharmacokinetic (PK) properties of a drug in a whole body system.

As master regulators of gene expression behind disease development and progression, some miRNAs may serve as therapeutic targets or agents (Bader et al., 2010; Kasinski and Slack, 2011; Ho and Yu, 2016). Among them, miR-34a is commonly downregulated in patient tumor tissues and acts as a tumor suppressor (see review (Bader, 2012)). Therefore, miR-34a agents may be reintroduced into tumor cells to control tumor progression and metastasis. Recently, our group has bioengineered a chimeric miR-34a agent and demonstrated this biologic miR-34a prodrug is effective to suppress miR-34a target gene expression, inhibit human carcinoma cell proliferation and invasion, and reduce tumor growth in subcutaneous and orthotopic xenograft mouse models

(Wang et al., 2015; Zhao et al., 2015; Zhao et al., 2016). However, it is unknown if therapeutic miR-34a would cause significant drug-drug interactions (DDI), which is a critical component in drug development, particularly for combination therapy.

A robust and relevant *in vivo* system is warranted for assessing PK DDI, rather than predictions using *in vitro* data. However, preclinical PK DDI studies have largely been limited to the use of larger animal species, such as rats, canines, and non-human primates. A major barrier to the use of mice for PK studies is attributable to the need for large volumes of blood collected at a sufficient number of individual time points to construct a robust, single-animal plasma drug concentration-time curve. As such, the use of mice in PK DDI studies has traditionally been limited to a "giant rat" approach, where individual mice are bled only at one to three time points and thus different mice are utilized to generate a complete blood drug concentration-time profile for naïve-pooled population PK analysis and modeling (Granvil et al., 2003; Shen et al., 2011; Jiang et al., 2013). This method is valid given a robust analytical technique; however, intra-individual variability may manifest in exacerbated inter-animal variation in the PK profile and estimated PK parameters, ultimately compromising statistical power.

To delineate the potential effects of miR-34a on PK of co-administered drugs or possible DDIs, we first established a new practical single-mouse PK approach, requiring only simple manual blood microsampling via mouse tail vein coupled to a sensitive and accurate LC-MS/MS assay. This LC-MS/MS assay allowed simultaneous quantification of five major CYP probe drugs and corresponding metabolites in minimal sample matrix. Complete plasma drug concentration-time curves in mice were thus successfully constructed and used for PK analyses. The validity and

DMD Fast Forward. Published on March 2, 2017 as DOI: 10.1124/dmd.116.074344
This article has not been copyedited and formatted. The final version may differ from this version.

utility of this single-mouse PK approach was further demonstrated by the sharp effects of selective CYP inhibitors and inducers on corresponding CYP probe drugs. Using this single-mouse PK approach we thus successfully defined the effects of miR-34a on PKs of individual CYP probe drugs.

Materials and Methods

Chemicals and Reagents. Chlorzoxazone (CLZ), α-naphthoflavone (α-NF), harmaline hydrochloride, 6-hydroxychlorzoxazone (6-OH-CLZ), ketoconazole (KTZ), 3-methylcholanthrene (3-MC), pregnenolone-16α-carbonitrile (PCN), phenacetin (PHE) and warfarin sodium were purchased from Sigma-Aldrich (St. Louis, MO). Acetaminophen (APAP) and ethylenediaminetetraacetic acid (EDTA) were purchased from MP Biomedicals, LLC (Aurora, OH). Dextromethorphan (DXM) hydrobromide and dextrophan (DXO) were purchased from ICN Biomedicals, Inc. (Aurora, OH). Diclofenac (DIC) sodium was purchased from TCI America (Portland, OR). Midazolam (MDZ) was purchased from Cambridge Isotope Laboratories (Tewksbury, MA). 1'-hydroxymidazolam (1'-OH-MDZ) was purchased from Bertin Pharma (Montigny le Bretonneux, France). 4'-hydroxydiclofenac (4'-OH-DIC) was purchased from Toronto Research Chemicals, Inc. (Toronto, ON, CA). Blank CD-1 mouse plasma (with EDTA) was purchased from BioreclamationIVT (Baltimore, MD). Sterile phosphate buffered saline (PBS, pH 7.4) was purchased from Gibco (Grand Island, NY). LC-MS grade acetonitrile (ACN), methanol, and formic acid were purchased from Fisher Scientific (Fair Lawn, NJ). In vivo jet-PEI was purchased from Polyplus-transfection (Illkirch, France).

The CYP probe substrate cocktail consisted of MDZ, PHE, DXM, DIC, and CLZ, and the stock solutions were dissolved in dimethyl sulfoxide. An appropriate dosing formulation was prepared by diluting the stock solutions into PBS for a dosage volume of 0.6 ml/30 g body weight and specific dose of 1.0 mg/kg MDZ, 2.8 mg/kg PHE, 26 mg/kg DXM, 3.25 mg/kg DIC, and 6.5 mg/kg CLZ.

DMD Fast Forward. Published on March 2, 2017 as DOI: 10.1124/dmd.116.074344
This article has not been copyedited and formatted. The final version may differ from this version.

Expression and Purification of RNA Agents. Recombinant miR-34a prodrug and the control tRNA/methionine-sephadex aptamer (tRNA/MSA) were prepared as previously described (Wang et al., 2015). Briefly, competent HST08 *Escherichia coli* were transformed with appropriate plasmids and following a 12-h incubation at 37 ℃, bacteria were pelleted, resuspended, lysed in phenol to extract total RNA, and precipitated with salt and ethanol. Target RNA was isolated from total RNAs by anion exchange fast protein liquid chromatography (FPLC) method using a NGC FPLC System (BioRad, Hercules, CA), and its purity (> 99%, data not shown) was verified by a HPLC assay (Wang et al., 2015).

Animals, Drug Administration, and Serial Blood Microsampling. All animal procedures were approved by the Institutional Animal Care and Use Committee at UC Davis and were carried out in accordance with the Guide for the Care and Use of Laboratory Animals (U. S. Department of Health and Human Services, 2015). 4-6 week-old male CD-1 mice (approximately 30 g bodyweight) were purchased from Charles River Laboratories (Hollister, CA), housed under 12 h light/dark conditions, and provided with diet and water *ad libitum*.

Mice were administered intraperitoneally (i.p.) with either KTZ (50 mg/kg) or α-NF (100 mg/kg) or vehicle (corn oil) (6 mice per group) to assess the impact of CYP inhibitor on probe drug PK. After 1 h, mice were given CYP probe substrate cocktail by oral gavage (p.o.) at specific doses outlined above. Immediately following cocktail administration, manual microsampling was conducted at the following time points: 3, 10, 20, 30, 45, 50, 90, 120, and 180 min. Specifically, a small volume of blood (10-20 μl) was collected by carefully inserting a 28-gauge needle pre-coated with 6% EDTA into the lateral tail vein of a mouse restrained by a mouse holder during blood

collection (Figure 1), mice were returned to their cages in between sampling time points. Mice were euthanized right after the experiment, and separate batches of mice were used for KTZ, α-NF and vehicle treatment groups. Blood was then transferred into a 1.5 ml microcentrifuge tube containing 1 μl of 6% EDTA, and centrifuged at 5,000 rpm and 4 ^{0}C for 10 min. Plasma was transferred into a clean microcentrifuge tube, and stored at -80 ^{0}C until LC-MS/MS quantification.

Likewise, different batches of mice were used to examine CYP inducer (6 mice per group) on the PK of CYP probe drugs, which were administered i.p. with either PCN (40 mg/kg), 3-MC (50 mg/kg), or vehicle (corn oil) once daily for 3 days. Cocktail administration and blood collection were conducted 24 h after the treatment with CYP inducer or vehicle and was conducted in the same manner as the inhibition study.

To assay the effects of miR-34a on systemic pharmacokinetics, a paired study design was followed using a separate cohort of mice which would improve statistical power. Mice were first administered i.v. with *in vivo*-jetPEI-formulated tRNA/MSA (15 μg of RNA, daily for four consecutive days). 24 h after the last dose of RNA agent, mice were treated with the CYP probe drug cocktail and blood samples were collected as described above. Following a two week washout and recovery period (U. S. Department of Health and Human Services, 2015), the same mice were injected with miR-34a prodrug using the same dose and regimen, followed by the PK study.

To examine the levels of miR-34a accumulation in mouse liver and impact on hepatic drug-metabolizing capacity, a separate batch of male CD-1 mice were administered either miR-34a agent or negative control (tRNA/MSA) using the same dosing scheme as described above. 24 h

DMD Fast Forward. Published on March 2, 2017 as DOI: 10.1124/dmd.116.074344
This article has not been copyedited and formatted. The final version may differ from this version.

following the final dose, mice were anesthetized and liver tissues were harvested for microsomal preparation. A small piece of liver tissue from each mouse was stored in RNAlater (Sigma-Aldrich) at -80 ℃ prior to RNA isolation.

LC-MS/MS Analysis of Cocktail Drugs and Corresponding Metabolites. Calibrators were prepared using blank CD-1 mouse plasma (with EDTA) and the appropriate concentrations of probe drugs and metabolites. Briefly, a 3 μl aliquot of calibrator or unknown plasma sample was added to 400 μl of acetonitrile containing 5 nM of internal standards warfarin and harmaline in a 1.5 ml microcentrifuge tube. To precipitate proteins, the tube was vortexed for 30 s and centrifuged at 13,200 rpm and 4 ^{0}C for 10 min. The supernatant was collected and dried over air at room temperature. The resulting residue was reconstituted with 60 μl of 20% methanol in distilled water and centrifuged at 13,200 rpm and 4 ^{0}C for 15 min to remove remaining debris prior to injection for LC-MS/MS analysis.

Drugs and metabolites were separated on a Zorbax C18 Eclipse Plus C18 reverse-phase LC column (2.1 × 50 mm, 3.5 μm; Agilent Technologies, Inc., Santa Clara, CA) maintained at 35 ^{0}C, using a Shimadzu Prominence Ultra-Fast Liquid Chromatography system (Shimadzu Corporation, Kyoto, Japan) consisted of binary pumps (LC-20AD), a degassing unit (LC-20A 3R), an autosampler (SIL-20AC HT), and a column oven (CTO-20AC). Mobile phases consisted of 100% water (A) and 100% methanol (B) supplemented with 0.1% formic acid (when used for ESI+ mode only). A constant flow rate of 0.4 ml/min was used for separation. In positive ion mode (ESI+) for the detection of MDZ, DXM, PHE and corresponding metabolites, column was eluted with 10% B for 0.5 min, which was increased to 25% B over 1.5 min, then to 45% B over 5 min, and then held at

90% B for 2 min before returned to initial condition for 3 min. In negative ion model (ESI-) for the analyses of CLZ, DIC and corresponding metabolites, column was eluted with 10% B for 1 min, which was increased to 52% B over 2.5 min, held at 52% B for 1.5 min, and then held at 90% B for 1 min before returned to initial conditions for 3 min.

Analytes were detected and quantified by multiple reaction monitoring (MRM) using an AB Sciex 4000 QTRAP tandem mass spectrometry system (AB Sciex, Framingham, MA) under an optimal condition: ion spray voltage of 5.4 kV, desolvation temperature of 500 ^{0}C curtain gas pressure of 30 psi, nebulizer and turbo gas pressures of 50 psi, and entrance potential of 10 V. Specific MS conditions for individual MRMs were optimized and are listed in Table 1. Each analyte peak area was normalized to the internal standard (harmaline for ESI+ analytes, and warfarin for ESI- analytes). Calibration curve was generated for each analyte using Analyst software (Version 1.6.2, AB Sciex). The accuracy and precision were further validated. In addition, following data analysis, analyte concentrations in a few test samples were revealed to be above the calibration ranges, which were accurately re-quantified after diluting the original plasma samples in blank CD-1 mouse plasma.

RNA Isolation and Quantification of pre-miR-34a and Mature miR-34a. Total RNA was isolated using Direct-zol RNA kit (Zymo Research, Irvine, CA), following the manufacturer's instructions. cDNA was generated by reverse transcription and levels of precursor and mature miR-34a were quantitated by corresponding selective real-time quantitative PCR assays on a CFX96 Touch real-time PCR system (Bio-Rad), as described previously (Wang et al., 2015). Cycle

DMD Fast Forward. Published on March 2, 2017 as DOI: 10.1124/dmd.116.074344
This article has not been copyedited and formatted. The final version may differ from this version.

thresholds for precursor and mature miR-34a were determined by regression, normalized to U6 small nucleolar RNA, and then to control using the $2^{-\Delta\Delta Ct}$ formula.

Mouse Liver Microsomes Preparation and *In Vitro* Drug Metabolism Incubation. Mouse liver microsomes were prepared by following the standard protocol (Knights et al., 2016) and protein concentrations were determined using a BCA Protein Assay Kit (Thermo Fisher Scientific Inc.).To assay intrinsic clearance of CYP probe drugs, microsomes (final concentration of 0.5 μg microsomal protein/μL in each incubation) were pre-incubated with CYP cocktail (final concentration of 3 μM PHE, 2 μM DXM, 1 μM MDZ, 2 μM DIC, and 3 μM CLZ) in 0.1 M potassium phosphate buffer, pH 7.4, in a water bath for 5 min at 37 ℃ . To initiate the reaction, NADPH (final concentration 1 mM) was added and the reaction was quenched at different time points (0, 5, 10, 20 min) with 3 mL ice cold acetonitrile containing 10 μM of harmaline and warfarin as internal standards. A negative control lacking NADPH was included alongside all samples and time points to determine enzymatic specificity and microsomes quality. The mixture was vortexed and centrifuged at 10,000 g for 10 min. 3 mL of supernatant was decanted and dried over air, and the residue was reconstituted with 100 μL of 20% methanol. Levels of parent drugs and specific metabolites were quantitated using the LC-MS/MS methods described above.

Pharmacokinetics Modeling. Pharmacokinetic data analyses were conducted using a non-compartmental model (Kinetica, Version 5.1, Thermo Fisher Scientific), which provided the estimation of corresponding PK parameters, maximum concentration (C_{max}), elimination half-life ($T_{1/2}$), area-under the plasma time curve ($AUC_{0\rightarrow\infty}$), extrapolated contribution to AUC (% Extrap), oral clearance (CL/F), and apparent volume of distribution during the terminal elimination phase

DMD Fast Forward. Published on March 2, 2017 as DOI: 10.1124/dmd.116.074344
This article has not been copyedited and formatted. The final version may differ from this version.

(V_z/F). In vitro substrate depletion data were fit to a mono-exponential decay model (or biphasic decay for MDZ). In vitro intrinsic clearance (CL_{int}) was calculated using the equation $CL_{int} = A_0/AUC_{0\rightarrow\infty}$.

Statistical Analysis. Values are means ± standard deviation. Drug and metabolite concentration versus time curves were compared for different treatments using two-way ANOVA and Bonferroni post-tests (GraphPad Prism, San Diego, CA). PK parameters were further compared using one-way ANOVA and Bonferroni post-tests. Difference was considered as statistically significant when the probability was less than 0.05 ($p < 0.05$).

DMD Fast Forward. Published on March 2, 2017 as DOI: 10.1124/dmd.116.074344
This article has not been copyedited and formatted. The final version may differ from this version.

Results

Validation of Single-Mouse PK Approach for DDI Study. Lateral tail vein puncture (Figure 1) was found to be a practical means to manual microsampling, yielding up to 20 µl of whole blood per time point. This procedure was found to cause minimal stress to the mice and a maximum of 180 µl of whole blood could be collected for 9 time points over a 3 h time period. Furthermore, following centrifugation and isolation of plasma, a small volume (3 µl) was found to be sufficient for LC-MS/MS quantification of multiple CYP probe drugs and corresponding metabolites under optimal MS conditions (Table 1). Calibrators fell within 15% variation were included to generate a calibration curve for each analyte, and all calibration curves showed excellent linearity ($R^2 \geq 0.99$) within the calibration ranges (Table 1). This LC-MS/MS assay provided accurate and precise quantification of both substrates and metabolites, with minimal intra- and inter-day variability (Table 2). As such, a complete PK profile was readily obtained after LC-MS/MS analyses of serial plasma samples obtained from single mouse (data not shown; Figures 2 and 3).

Single-Mouse PK Studies on Inhibition Based DDI. To evaluate utility of this single-mouse PK method, we first examined the effects of KTZ and α-NF, two known CYP inhibitors, on the PKs of individual CYP probe substrates in mice. The results showed that plasma MDZ concentrations were significantly increased in mice pretreated with KTZ, which was reflected by a two- or three-fold increase in both C_{max} and $AUC_{0\rightarrow\infty}$, respectively, lower oral clearance CL/F, and prolonged elimination $t_{1/2}$ (Table 3). This was also associated with significantly lower levels of 1'-OH-MDZ in mice pretreated with KTZ (Figure 2; Table 3). By contrast, plasma MDZ and 1'-OH-MDZ

DMD Fast Forward. Published on March 2, 2017 as DOI: 10.1124/dmd.116.074344
This article has not been copyedited and formatted. The final version may differ from this version.

concentrations and PK parameters were not significantly affected by α-NF pretreatment, with respect to control (Figure 2 and Table 3).

Pretreatment with α-NF led to significant higher plasma PHE concentrations in mice (Figure 2), and this was reflected by a two-fold increase in AUC and $t_{1/2}$, as well as reduction in clearance by one-half (Table 3). Consistently, plasma APAP concentrations were significantly lower in mice pretreated with α-NF (Figure 2), which was also indicated by significantly lower C_{max} and $AUC_{0\rightarrow\infty}$ values (Table 3). Interestingly, plasma PHE concentrations in KTZ-treated mice showed a general decrease as compared to control (Figure 2), reflected in a significantly decreased C_{max} and $AUC_{0\rightarrow\infty}$ and increased apparent volume of distribution V_z/F (Table 3). Nevertheless, mouse plasma APAP concentrations were not affected by KTZ treatment.

As expected, neither KTZ nor α-NF treatment had significant impact on mouse plasma DXM concentrations and PK parameters (Figure 2 and Table 3). However, plasma DXO concentrations were significantly lower in KTZ-treated mice, particularly at earlier time points (Figure 2), which was indicated by lower C_{max} and $AUC_{0\rightarrow\infty}$ values (Table 3). In addition, α-NF treatment did not alter DIC and CLZ PK in mice, whereas KTZ surprisingly caused a significant higher systemic exposure to DIC and CLZ (Figure 2 and Table 3). Inhibition of DIC and CLZ clearance was also associated with lower levels of exposure to their metabolites, 4'-OH-DIC and 6-OH-CLZ, respectively, in KTZ-treated mice (Figure 2 and Table 3).

Single-Mouse PK Studies on Induction Based DDI. We further employed this single-mouse PK method to investigate the effects of PCN and 3-MC, two known CYP inducers, on the PKs of

DMD Fast Forward. Published on March 2, 2017 as DOI: 10.1124/dmd.116.074344
This article has not been copyedited and formatted. The final version may differ from this version.

individual CYP probe substrates in mice. The results showed that plasma MDZ concentrations were sharply reduced in PCN-induced mice (Figure 3), which was manifested by an 8-fold reduction in C_{max} values and 24-fold decrease of $AUC_{0\rightarrow\infty}$ values (Table 4). Surprisingly, plasma unconjugated 1'-OH-MDZ concentrations were not increased but decreased by almost 10-fold at later time points in PCN-treated mice, leading to a 6-fold lower $AUC_{0\rightarrow\infty}$ and 2-fold lower $t_{1/2}$ value. In addition, pretreatment of 3-MC significantly decreased systemic exposure to MDZ as compared to the control, whereas the degrees of change in PK parameters such as C_{max}, $AUC_{0\rightarrow\infty}$, and CL/F were reduced when compared to PCN treatment (Figure 3 and Table 4).

Compared to the control, pretreated with 3-MC remarkably reduced plasma PHE concentrations in mice, whereas PCN showed minimal effects (Figure 3). In particular, plasma PHE concentrations in 3-MC-treated animals were reduced by approximately 10-fold at all time points, and then fell below the lowest limit of quantification (Table 1) at 45 minutes compared with 60 minutes for control and PCN-treated groups, similar to the observation for MDZ in PCN-treated animals (Figure 3). As such, there were 6- and 33-fold decreases in C_{max} and $AUC_{0\rightarrow\infty}$ values in 3-MC-treated mice (Table 4), respectively. Likewise, plasma unconjugated APAP concentrations were reduced in both PCN- and 3-MC-treated animals with respect to control, although to a slightly greater degree in 3-MC-treated mice (Figure 3 and Table 4).

In addition, pretreatment of PCN and 3-MC significantly reduced plasma DXM, DIC, and CLZ concentrations in mice (Figure 3), despite that to a lower degree than the effects of PCN on MDZ or 3-MC on PHE. This was also manifested by modest changes of PK parameters including the decrease of C_{max} and $AUC_{0\rightarrow\infty}$ values, as well as the increase of CL/F values (Table 4). However,

DMD Fast Forward. Published on March 2, 2017 as DOI: 10.1124/dmd.116.074344
This article has not been copyedited and formatted. The final version may differ from this version.

the effects of PCN and 3-MC on unconjugated metabolite levels were relatively complex (Figure 3). Firstly, DXO concentrations were lower in PCN- and 3-MC-treated mice at all time points. Secondly, 4-OH-DIC concentrations were generally lower in 3-MC-treated mice at all time points, whereas they were higher in PCN-treated mice at earlier stage (0-30 min) and much lower at later stage (30-180 min). Thirdly, PCN treatment led to the production of significantly higher levels of plasma 6-OH-CLZ concentrations in mice, while 3-MC showed minimal influence. These effects were consistently reflected in the changes of corresponding PK parameters such as C_{max}, $AUC_{0\rightarrow\infty}$, and $t_{1/2}$ (Table 4).

Effects of Biologic miR-34a Agent on the PK of CYP Probe Drugs. Following the validation of this single-mouse PK method through inhibition and induction based DDI studies we examined possible impact of miR-34a on the PKs of individual CYP probe substrates in mice. As shown by the drug concentrations versus time profiles (Figure 4) and PK parameters (Table 5), pre-treatment of miR-34a had no or minimal effects on the PK of PHE, DXM and CLZ as well as their corresponding metabolites, whereas a modest impact on the PK of MDZ and DIC. In particular, the $AUC_{0\rightarrow\infty}$ of MDZ was 60% higher in mice treated with miR-34a than the control, while its elimination $t_{1/2}$ and primary PK parameters were unaffected. Furthermore, there was no difference in 1'-OH-MDZ PK in mice treated with miR-34a and control RNA. Similarly, a higher C_{max} of DIC was observed in mice following miR-34a pre-treatment (Figure 4), leading to a 10% higher exposure ($AUC_{0\rightarrow\infty}$) which was rather not statistically significant (Table 5). Likewise, the PK of metabolite 4'-OH-DIC did not differ in mice treated with miR-34a and control RNA. These findings indicated that miR-34a seemed to have a marginal (<50%) impact on the PK of CYP probe drugs in mice as compared to control RNA.

DMD Fast Forward. Published on March 2, 2017 as DOI: 10.1124/dmd.116.074344
This article has not been copyedited and formatted. The final version may differ from this version.

The levels of precursor and mature miR-34a were found to be increased by approximately 10- and 80-fold, respectively, in mouse livers treated with biologic miR-34a prodrug (Figure 5A), which indicate hepatic accumulation of pre-miR-34a and production of mature miR-34a. Additionally, time-dependent substrate depletion was found to be minimally altered by liver microsomes prepared from the mice treated with miR-34a agent, as compared to the control (Figure 5B). Notably, DXM depletion (CL_{int}) was attenuated by approximately 30% in liver microsomes derived from miR-34a-treated mice. Finally, the depletion of DIC and CLZ depletion was revealed to be minimal in mouse liver microsomes prepared from both groups (Figure 5B), and both were indistinguishable from the NADPH-null reaction controls (data not shown), which agree with their metabolic stabilities in liver microsomes.

DMD Fast Forward. Published on March 2, 2017 as DOI: 10.1124/dmd.116.074344
This article has not been copyedited and formatted. The final version may differ from this version.

Discussion

With the development of new carriers for the delivery of nucleic acids, many RNA agents have entered clinical trials as drug candidates (Ho and Yu, 2016). Because some miRNAs regulate genes underlying drug metabolism and disposition (Yu, 2009; Ingelman-Sundberg et al., 2013; Yokoi and Nakajima, 2013; Yu et al., 2016), for safety reasons, it is essential to evaluate possible DDI *in vivo*. Recently, our group has engineered a biologic miR-34a prodrug whose mechanistic actions on target gene expression and xenograft tumor progression have been documented (Wang et al., 2015; Zhao et al., 2015; Zhao et al., 2016). In the present study, we elucidated the effects of biologic miR-34a on the PKs of five CYP probe drugs following the establishment and validation of a general, rapid, and practical single-mouse PK approach. Our results demonstrated a rather marginal (45-48%) influence of miR-34a on systemic exposure to midazolam and diclofenac in mouse models, as well as the lack of effects on PKs of dextromethorphan, phenacetin and chlorzoxazone.

This single-mouse PK approach involves a simple (non-)terminal, manual serial microsampling procedure whereas it requires a sensitive and accurate LC-MS/MS analytical assay. Tail vein blood collection has been proved to be a reliable means for PK studies in rodents. A thorough comparison of PKs of six marketed drugs in rats using tail vein, cannula and retro-orbital bleeding methods demonstrated that there were no or minor differences in PK properties among these blood sampling methods (Hui et al., 2007). Although one study reported statistically significant differences in gabapentin PK parameters (e.g., oral bioavailability: 46.82 ± 19.45% versus 61.54 ± 21.23%) in rats for manual and automated blood sampling methods (Aryal et al., 2011) and the latter

procedures could be less stressful to mice (Teilmann et al., 2014), the actual 1.3-fold difference was rather marginal. Most importantly, the plasma drug concentrations versus time curves and estimated PK parameters using this single-mouse PK approach were equally or less variable than those studies using "giant rat" models (Granvil et al., 2003; Shen et al., 2011; Jiang et al., 2013), and variabilities shown in single-mouse PK studies should represent true differences among individual subjects.

The robustness and application of this single-mouse PK approach is demonstrated by the degrees of mechanistic DDIs between selective CYP inhibitors/inducers and corresponding CYP probe drugs in CD-1 mice. Supporting this, we found that pretreatment of α-NF led to a 2.3-fold increase of systemic exposure to PHE, and pretreatment of 3-MC resulted in a 33-fold decrease of exposure to PHE, which are in general agreement with those values identified using rat models (Table 7) while variable drug dosing regimens and animal models may provide some explanations for inter-study variations. The 2.8-fold increase of systemic exposure to MDZ in a single dose of KTZ-treated CD-1 mice revealed in the present study is also close to the 3.3-fold increase defined in FVB/N mice (Granvil et al., 2003), given some rather minor differences in the stains of mice, doses of KTZ and MDZ, routes of administration, and dosing interval (Table 7). Inter-study variations are also obvious for the degrees of DDIs between MDZ and KTZ in humans, where single dose of KTZ showed reasonably less impact on MDZ exposure as compared to multiple doses of KTZ (Table 7). Furthermore, the sharp change of MDZ exposure (25-fold decrease) in PCN-treated mice defined by single-mouse PK approach in the present study supports the selectivity of PCN to induce murine drug-metabolizing enzymes via the activation of murine pregnane X receptor (PXR) and the critical role of intestinal enzymes in the control of PK of orally administered MDZ

(McCrea et al., 1999; Tsunoda et al., 1999; Granvil et al., 2003; Lam et al., 2003; Pang et al., 2011). Finally, as Phase 2 conjugation metabolites are not monitored using this assay, a significant decrease rather than increase in plasma 1'-OH-MDZ concentration was observed in mice administered PCN. This is most likely explained by further conjugations of 1'-OH-MDZ, as mouse UDP-glucuronosyltransferases are inducible following PCN-mediated activation of PXR (Buckley and Klaassen, 2009).

The effects of CYP inducers (PCN and 3-MC), as well as CYP inhibitors (KTZ and α-NF), on the PK properties of parent probe drugs (e.g., MDZ and PHE) revealed in the present study not only highlights the importance of corresponding murine Cyp enzymes in the metabolism of these drugs but also illustrates some species differences. For example, lower levels of DDI between KTZ and MDZ in mice than humans (Table 7) may be in part due to significant contribution of Cyp2c enzymes to MDZ 1'-hydroxylation in mice (Perloff et al., 2000). In addition, we observed an approximately equal level of decrease in APAP exposure in KTZ- and α-NF-treated mice, whereas substrate drug PHE concentrations were decreased in KTZ-treated mice and increased in α-NF-treated mice. Likewise, nearly equal significant decrease in APAP exposure was found in both PCN- and 3-MC-treated mice, whereas PHE concentrations were only decreased in 3-MC-treated mice. While the exact mechanisms are unknown, the decrease in APAP may be partially due to complex changes of Phase 2 conjugations following PHE *O*-deethylation, as well as the involvement of various Cyp enzymes in APAP metabolism (Patten et al., 1993; Zaher et al., 1998). The observed increase in the exposure to DIC by KTZ (Figure 2) may be interpreted by the fact that DIC is oxidized not only by Cyp2c enzymes but also other CYP isoforms including Cyp3a in mice (Tang et al., 1999; Scheer et al., 2012). In addition, DXO formation was decreased about 2-

fold in KTZ-treated mice and DXM PK were coincidentally altered, which may reflect a modest inhibition of murine DXM *O*-demethylase Cyp2d enzymes by KTZ (Yu and Haining, 2006).

Using this single-mouse PK approach and a biologic miR-34a agent, rather than synthetic miRNA reagents bearing extensive artificial modifications (Duan and Yu, 2016; Ho and Yu, 2016), we were able to identify the somewhat limited effects of miR-34a on PK of individual CYP probe drugs; this was also supported by findings from in vitro metabolism study. Compared to control RNA treatment, miR-34a either did not affect (e.g., DXM, PHE and CLZ exposure) or led to minor (<50%) changes (e.g., MDZ and DIC). Compared to control, DIC C_{max} and MDZ $AUC_{0\rightarrow\infty}$ values in miR-34a-treated mice were significantly increased (Table 5), suggesting possible alteration of murine Cyp3a and Cyp2c by miR-34a. This is complementary to studies that found negative correlation between miR-34a and CYP3A4 and 2C19 (Lamba et al., 2014), as well as miR-34a targeting of RXRα/NR2B1 (Oda et al., 2014) and Nrf2/NFE2L2 (Huang et al., 2014) by miR-34a. In addition, the transcription factor HNF4α has been found to be highly conserved between mouse and human species (Boj et al., 2009) and miRNA recognition elements have been identified for miR-34a in both human and mouse 3'UTR of HNF4α mRNA (Takagi et al., 2010) (three miR-34a MREs within murine Rxra 3'UTR by TargetScan (http://www.targetscan.org) and miRanda (http://www.microrna.org)).

Our findings from mouse models are also complicated by the presence of species differences in the expression of regulatory factors, and drug-metabolizing enzymes and transporters as well as their functions in processing the drugs. Indeed, the present study found that the formation of both 1'-OH-MDZ or 4'-OH-DIC were not altered *in vivo* (Table 5), nor was CL_{int} of either parent drug

affected *in vitro* (Table 6). These data suggest that miR-34a-induced alterations to MDZ or DIC PK are not manifested in alteration of murine Cyp enzymes. Additionally, DIC and CLZ depletion in mouse liver microsomes (Figure 5B) was minimal, which not only supports their metabolic stability in microsomes but also suggests the presence of other mechanisms besides hepatic microsomal metabolism that are responsible for their clearance. As such, the discrepancy between the observed alterations to *in vivo* PK and *in vitro* probe drug clearance may be explained by modulation of phase II enzyme or drug transporter genes by miR-34a. Indeed, RXRα, a putative miR-34a target, likely modulates the expression of several glutathione S-transferase isoforms (Dai et al., 2005), although no similar evidence exists for sulfo- or glucuronosyltransferase enzymes.

In summary, this study established a practical approach to perform single-mouse PK and DDI studies which was employed to demonstrate the remarkable PK DDIs between selective CYP inhibitors/inducers and CYP probe drugs in mice, as well as some species differences. In addition, we were able to reveal the marginal effects of miR-34a on MDZ, DIC, and DXM PK in mice. However, further research is required to confirm the findings, particularly in a more translational humanized mouse model.

Acknowledgments

The authors would like to thank Pui Yan Ho, Meijuan Tu, and Cindy McReynolds for assistance in processing blood samples during the pharmacokinetics studies.

Authorship Contributions

Participated in research design: Yu, Jilek, and Tian.

Conducted experiments: Jilek and Tian.

Performed data analysis: Jilek and Tian.

Wrote or contributed to the writing and revision of the manuscript: Jilek, Tian and Yu.

Contributed equally to this study: Jilek and Tian

References

Ambros V (2004) The functions of animal microRNAs. *Nature* **431:**350-355.

Aryal B, Tae-Hyun K, Yoon-Gyoon K, and Hyung-Gun K (2011) A comparative study of the pharmacokinetics of traditional and automated dosing/blood sampling systems using gabapentin. *Indian J Pharmacol* **43:**262-269.

Bader AG (2012) miR-34 - a microRNA replacement therapy is headed to the clinic. *Front Genet* **3:**120.

Bader AG, Brown D, and Winkler M (2010) The promise of microRNA replacement therapy. *Cancer Res* **70:**7027-7030.

Boj SF, Servitja JM, Martin D, Rios M, Talianidis I, Guigo R, and Ferrer J (2009) Functional targets of the monogenic diabetes transcription factors HNF-1alpha and HNF-4alpha are highly conserved between mice and humans. *Diabetes* **58:**1245-1253.

Buckley DB and Klaassen CD (2009) Induction of mouse UDP-glucuronosyltransferase mRNA expression in liver and intestine by activators of aryl-hydrocarbon receptor, constitutive androstane receptor, pregnane X receptor, peroxisome proliferator-activated receptor alpha, and nuclear factor erythroid 2-related factor 2. *Drug Metab Dispos* **37:**847-856.

Dai G, Chou N, He L, Gyamfi MA, Mendy AJ, Slitt AL, Klaassen CD, and Wan YJ (2005) Retinoid X receptor alpha Regulates the expression of glutathione s-transferase genes and modulates acetaminophen-glutathione conjugation in mouse liver. *Mol Pharmacol* **68:**1590-1596.

Duan Z and Yu AM (2016) Bioengineered non-coding RNA agent (BERA) in action. *Bioengineered***:**1-7.

Granvil CP, Yu AM, Elizondo G, Akiyama TE, Cheung C, Feigenbaum L, Krausz KW, and Gonzalez FJ (2003) Expression of the human CYP3A4 gene in the small intestine of transgenic mice: in vitro metabolism and pharmacokinetics of midazolam. *Drug Metab Dispos* **31:**548-558.

Ho PY and Yu AM (2016) Bioengineering of noncoding RNAs for research agents and therapeutics. *Wiley interdisciplinary reviews RNA* **7:**186-197.

Huang X, Gao Y, Qin J, and Lu S (2014) The role of miR-34a in the hepatoprotective effect of hydrogen sulfide on ischemia/reperfusion injury in young and old rats. *PLoS One* **9:**e113305.

Hui YH, Huang NH, Ebbert L, Bina H, Chiang A, Maples C, Pritt M, Kern T, and Patel N (2007) Pharmacokinetic comparisons of tail-bleeding with cannula- or retro-orbital bleeding techniques in rats using six marketed drugs. *J Pharmacol Toxicol Methods* **56:**256-264.

Ingelman-Sundberg M, Zhong XB, Hankinson O, Beedanagari S, Yu AM, Peng L, and Osawa Y (2013) Potential role of epigenetic mechanisms in the regulation of drug metabolism and transport. *Drug Metab Dispos* **41:**1725-1731.

Jiang XL, Shen HW, Mager DE, and Yu AM (2013) Pharmacokinetic interactions between monoamine oxidase A inhibitor harmaline and 5-methoxy-N,N-dimethyltryptamine, and the impact of CYP2D6 status. *Drug Metab Dispos* **41:**975-986.

Kasinski AL and Slack FJ (2011) Epigenetics and genetics. MicroRNAs en route to the clinic: progress in validating and targeting microRNAs for cancer therapy. *Nat Rev Cancer* **11:**849-864.

Klippert PJ, Littel RJ, and Noordhoek J (1983) In vivo O-de-ethylation of phenacetin in 3-methylcholanthrene-pretreated rats: gut wall and liver first-pass metabolism. *The Journal of pharmacology and experimental therapeutics* **225:**153-157.

Knights KM, Stresser DM, Miners JO, and Crespi CL (2016) In Vitro Drug Metabolism Using Liver Microsomes. *Curr Protoc Pharmacol* **74:**7 8 1-7 8 24.

Kotegawa T, Laurijssens BE, Von Moltke LL, Cotreau MM, Perloff MD, Venkatakrishnan K, Warrington JS, Granda BW, Harmatz JS, and Greenblatt DJ (2002) In vitro, pharmacokinetic, and pharmacodynamic interactions of ketoconazole and midazolam in the rat. *The Journal of pharmacology and experimental therapeutics* **302:**1228-1237.

Lam YW, Alfaro CL, Ereshefsky L, and Miller M (2003) Pharmacokinetic and pharmacodynamic interactions of oral midazolam with ketoconazole, fluoxetine, fluvoxamine, and nefazodone. *J Clin Pharmacol* **43:**1274-1282.

Lamba V, Ghodke Y, Guan W, and Tracy TS (2014) microRNA-34a is associated with expression of key hepatic transcription factors and cytochromes P450. *Biochem Biophys Res Commun* **445:**404-411.

McCrea J, Prueksaritanont T, Gertz BJ, Carides A, Gillen L, Antonello S, Brucker MJ, Miller-Stein C, Osborne B, and Waldman S (1999) Concurrent administration of the erythromycin breath test (EBT) and oral midazolam as in vivo probes for CYP3A activity. *J Clin Pharmacol* **39:**1212-1220.

Oda Y, Nakajima M, Tsuneyama K, Takamiya M, Aoki Y, Fukami T, and Yokoi T (2014) Retinoid X receptor alpha in human liver is regulated by miR-34a. *Biochemical pharmacology* **90:**179-187.

Pang X, Cheng J, Krausz KW, Guo DA, and Gonzalez FJ (2011) Pregnane X receptor-mediated induction of Cyp3a by black cohosh. *Xenobiotica* **41:**112-123.

Patten CJ, Thomas PE, Guy RL, Lee M, Gonzalez FJ, Guengerich FP, and Yang CS (1993) Cytochrome P450 enzymes involved in acetaminophen activation by rat and human liver microsomes and their kinetics. *Chem Res Toxicol* **6:**511-518.

Perloff MD, von Moltke LL, Court MH, Kotegawa T, Shader RI, and Greenblatt DJ (2000) Midazolam and triazolam biotransformation in mouse and human liver microsomes: relative contribution of CYP3A and CYP2C isoforms. *The Journal of pharmacology and experimental therapeutics* **292:**618-628.

Scheer N, Kapelyukh Y, Chatham L, Rode A, Buechel S, and Wolf CR (2012) Generation and characterization of novel cytochrome P450 Cyp2c gene cluster knockout and CYP2C9 humanized mouse lines. *Mol Pharmacol* **82:**1022-1029.

Shen HW, Jiang XL, and Yu AM (2011) Nonlinear pharmacokinetics of 5-methoxy-N,N-dimethyltryptamine in mice. *Drug Metab Dispos* **39:**1227-1234.

Takagi S, Nakajima M, Kida K, Yamaura Y, Fukami T, and Yokoi T (2010) MicroRNAs regulate human hepatocyte nuclear factor 4alpha, modulating the expression of metabolic enzymes and cell cycle. *The Journal of biological chemistry* **285:**4415-4422.

Tang W, Stearns RA, Bandiera SM, Zhang Y, Raab C, Braun MP, Dean DC, Pang J, Leung KH, Doss GA, Strauss JR, Kwei GY, Rushmore TH, Chiu SH, and Baillie TA (1999) Studies on cytochrome P-450-mediated bioactivation of diclofenac in rats and in human hepatocytes: identification of glutathione conjugated metabolites. *Drug Metab Dispos* **27:**365-372.

Teilmann AC, Kalliokoski O, Sorensen DB, Hau J, and Abelson KS (2014) Manual versus automated blood sampling: impact of repeated blood sampling on stress parameters and behavior in male NMRI mice. *Lab Anim* **48:**278-291.

Tsunoda SM, Velez RL, von Moltke LL, and Greenblatt DJ (1999) Differentiation of intestinal and hepatic cytochrome P450 3A activity with use of midazolam as an in vivo probe: effect of ketoconazole. *Clin Pharmacol Ther* **66:**461-471.

U. S. Department of Health and Human Services NIoH, Office of Animal Care and Use (2015) Guidelines for Survival Bleeding of Mice and Rats. *Retrieved from http://oacuodnihgov/ARAC/documents/Rodent_Bleedingpdf*.

Wang WP, Ho PY, Chen QX, Addepalli B, Limbach PA, Li MM, Wu WJ, Jilek JL, Qiu JX, Zhang HJ, Li T, Wun T, White RD, Lam KS, and Yu AM (2015) Bioengineering Novel Chimeric microRNA-34a for Prodrug Cancer Therapy: High-Yield Expression and Purification, and Structural and Functional Characterization. *The Journal of pharmacology and experimental therapeutics* **354:**131-141.

Yokoi T and Nakajima M (2013) microRNAs as mediators of drug toxicity. *Annu Rev Pharmacol Toxicol* **53:**377-400.

Yu AM (2009) Role of microRNAs in the regulation of drug metabolism and disposition. *Expert Opin Drug Metab Toxicol* **5:**1513-1528.

Yu AM and Haining RL (2006) Expression, purification, and characterization of mouse CYP2d22. *Drug Metab Dispos* **34:**1167-1174.

Yu AM, Tian Y, Tu MJ, Ho PY, and Jilek JL (2016) MicroRNA Pharmacoepigenetics: Posttranscriptional Regulation Mechanisms behind Variable Drug Disposition and Strategy to Develop More Effective Therapy. *Drug Metab Dispos* **44:**308-319.

Zaher H, Buters JT, Ward JM, Bruno MK, Lucas AM, Stern ST, Cohen SD, and Gonzalez FJ (1998) Protection against acetaminophen toxicity in CYP1A2 and CYP2E1 double-null mice. *Toxicol Appl Pharmacol* **152:**193-199.

Zhao Y, Tu MJ, Wang WP, Qiu JX, Yu AX, and Yu AM (2016) Genetically engineered pre-microRNA-34a prodrug suppresses orthotopic osteosarcoma xenograft tumor growth via the induction of apoptosis and cell cycle arrest. *Sci Rep* **6:**26611.

Zhao Y, Tu MJ, Yu YF, Wang WP, Chen QX, Qiu JX, Yu AX, and Yu AM (2015) Combination therapy with bioengineered miR-34a prodrug and doxorubicin synergistically suppresses osteosarcoma growth. *Biochemical pharmacology* **98:**602-613.

Zhuang XM, Zhong YH, Xiao WB, Li H, and Lu C (2013) Identification and characterization of psoralen and isopsoralen as potent CYP1A2 reversible and time-dependent inhibitors in human and rat preclinical studies. *Drug Metab Dispos* **41:**1914-1922.

DMD Fast Forward. Published on March 2, 2017 as DOI: 10.1124/dmd.116.074344
This article has not been copyedited and formatted. The final version may differ from this version.

Footnotes

Sources of Financial Support: This work was supported by grants from The National Institute of General Medical Sciences [R01GM133888] and National Cancer Institute [U01CA175315], National Institutes of Health. JLJ was supported by a NIGMS-funded Pharmacology Training Program grant [T32GM099608].

Send reprint requests to: Prof. Ai-Ming Yu, Department of Biochemistry & Molecular Medicine, UC Davis School of Medicine, 2700 Stockton Boulevard, Sacramento, CA 95817, USA. E-mail: aimyu@ucdavis.edu.

DMD Fast Forward. Published on March 2, 2017 as DOI: 10.1124/dmd.116.074344
This article has not been copyedited and formatted. The final version may differ from this version.

Figure Legends

Figure 1: Serial blood microsampling from single mouse. Mouse was restrained using a cylinder, allowing free access to the tail. (**A**) Using a 30 gauge needle, the lateral tail vein was pierced at an angle similar to intravenous injection into the tail vein. The plunger of the syringe was slightly aspirated and needle was quickly removed and a large drop of blood was allowed to form, using pressure to draw blood to the site of puncture if necessary. (**B**) The drop of blood was quickly collected using a 10 μl pipette tip (previously coated with 6% EDTA), transferred to a microcentrifuge tube containing 1 μl 6% EDTA, and placed on ice until centrifugation.

Figure 2: Single-mouse PK profiles of multiple CYP probe drugs and corresponding metabolites - Effects of known CYP inhibitors. Pre-treatment with a single 50 mg/kg i.p. dose of KTZ led to a sharply increased systemic exposure to midazolam as well as significantly higher exposure to diclofenac and chlozoxazone. By contrast, a single 100 mg/kg i.p. dose of α-NF prior to cocktail administration caused much higher exposure to phenacetin. Two-way ANOVA with Bonferroni post-hoc tests: $p < 0.001$ for drug treatment and time; $^{***}p < 0.001$, $^{**}p < 0.01$, and $^{*}p < 0.05$ at indicated time points, compared to vehicle control. Mice were pretreated i.p. with KTZ, α-NF, or vehicle. One hour later, the cocktail drugs were administered via oral gavage, setting t = 0 min. Blood collection was carried out over 3-180 min. Data at individual time points represent mean ± SD of 6 animals, as determined by LC-MS/MS assay. Missing data for some treatments at later time points were noted when analyte concentrations from all animals fell below the lower limits of quantification of the analytical assay.

Figure 3: Single-mouse PK profiles of multiple CYP probe drugs and corresponding metabolites - Effects of known CYP inducers. Pre-treatment with three 40 mg/kg i.p. doses (24 h apart) of PCN led to a remarkable lower exposure to midazolam and chlozoxazone; similarly, three 50 mg/kg i.p. doses of 3-MC sharply reduced the exposure to phenacetin, midazolam, and chlorzoxazone. Slight decrease in systemic exposure to dextromethorphan and diclofenac was also shown in PCN- and 3-MC-treated mice. Two-way ANOVA with Bonferroni post-hoc tests: $p < 0.001$ for drug treatment and time; ***$p < 0.001$, **$p < 0.01$, and *$p < 0.05$ at indicated time points, compared to vehicle control. Mice were administered i.p. either PCN, 3-MC, or vehicle (corn oil) every day for three days. One day following the final dose, animals were administered the cocktail drugs by oral gavage (setting t = 0 min) and blood was collected over 3-180 min. Data are mean ± SD of 6 animals. Missing data for some treatments at later time points were noted when analyte concentrations from all animals fell below the lower limits of quantification of the analytical assay.

Figure 4: Effects of miR-34a on PK profiles of individual CYP probe drugs and corresponding metabolites. Intravenous administration of miR-34a (15 µg/mouse, dosed 4 times over 4 days) to mice led to 45% and 48% increase in systemic exposure to midazolam and diclofenac, respectively. Mice were treated i.v. with miR-34a for four days, followed by oral administration of cocktail drugs. Following a two-week wash-out and recovery period, the same mice were pre-treated i.v. with control tRNA/MSA for four days, followed by oral administration of the cocktail drugs. Individual data points represent mean ± SD of 6 mice. ***$p < 0.001$, **$p < 0.01$, and *$p < 0.05$ at indicated time points, compared to control treatment (Two-way ANOVA with paired Bonferroni post-hoc tests).

DMD Fast Forward. Published on March 2, 2017 as DOI: 10.1124/dmd.116.074344
This article has not been copyedited and formatted. The final version may differ from this version.

Figure 5: Clearance of CYP probe drugs by liver microsomes prepared from mice treated with miR-34a and control RNA. (**A**) Precursor and mature miR-34a levels were significantly higher in liver tissues of mice treated with bioengineered miR-34a prodrug. Mature miR-34a and pre-miR-34a were quantitated by selective qPCR assays and normalized to U6. (**B**) Comparison of the activities of mouse liver microsomes in the clearance of CYP probe drugs. Mice (five per treatment group) were treated i.v. with miR-34a or control RNA for four days. Total RNA and microsomes were prepared from dissected liver tissues for qPCR and in vitro metabolism experiments, respectively. Data represent mean ± SD (N = 5 per group). ***$p < 0.001$, **$p < 0.01$, and *$p < 0.05$ at indicated time points, compared to control (A, unpaired t test; B, 2-way ANOVA with Bonferroni post-hoc tests).

Table 1. ESI-MS/MS conditions and calibration ranges for individual analytes. Analytes were separated on a C18 column prior to positive or negative ESI MRM of each analyte. DP, declustering potential; CE, collision energy; CXP, collision cell exit potential; mSec, millisecond. Calibrators were standard drugs and metabolites spiked in blank CD-1 mouse plasma and processed as described in Methods.

Analyte	Retention Time (min)	ESI Mode	MRM Transition (Da)	Scan Time (mSec)	DP (V)	CE (V)	CXP (V)	Calibration Range (nM)
Phenacetin	5.81	ESI+	180.0→110.1	150	61	29	8	25 – 5000
Acetaminophen	1.26	ESI+	152.1→110.1	130	41	27	8	5 – 1000
Dextromethorphan	7.13	ESI+	272.3→171.1	150	91	57	14	25 – 5000
Dextrophan	4.33	ESI+	258.2→157.0	100	51	53	12	5 – 1000
Midazolam	6.97	ESI+	326.7→292.1	150	81	41	8	5 – 1000
1'-OH-Midazolam	7.34	ESI+	342.0→203.0	150	51	35	10	25 – 5000
Harmaline (IS)	4.89	ESI+	215.2→172.1	110	36	43	16	---
Diclofenac	6.93	ESI-	294.0→249.8	300	-55	-16	-5	25 – 5000
4'-OH-Diclofenac	6.50	ESI-	309.9→265.7	200	-55	-16	-7	5 – 1000
Chlorzoxazone	5.28	ESI-	167.8→131.9	200	-60	-28	-5	25 – 5000
6'-OH-Chlorzoxazone	3.64	ESI-	183.8→119.9	150	-55	-26	-7	5 – 1000
Warfarin (IS)	6.57	ESI-	306.8→160.9	100	-60	-28	-11	---

Table 2. Intra- and inter-day precision and accuracy for LC-MS/MS quantification of CYP probe drugs and corresponding metabolites in mouse plasma. SD, standard deviation; RSD, relevant standard deviation.

Analyte	Nominal Concentration	Intra-Assay (n = 3) Measured Concentration	RSD (%)	Accuracy (%)	Inter-Assay (n = 9) Measured Concentration	RSD (%)	Accuracy (%)
Phenacetin	75	69.93 ± 18.70	26.7	93.2	75.69 ± 10.84	14.3	101
	400	387.7 ± 20.8	5.38	96.8	394.9 ± 15.4	3.89	98.6
	4000	3580 ± 114	3.17	89.4	3707 ± 168	4.54	92.6
Acetaminophen	15	14.97 ± 1.85	12.4	99.9	15.69 ± 1.23	7.84	104
	80	81.57 ± 0.96	1.18	102	78.96 ± 2.38	3.02	98.7
	800	699.7 ± 11.8	1.69	87.4	722.6 ± 36.5	5.05	90.3
Midazolam	15	15.40 ± 1.95	12.7	103	14.63 ± 1.98	13.6	97.5
	80	73.77 ± 5.13	6.95	92.2	77.96 ± 9.29	11.9	97.4
	800	688.7 ± 66.3	9.62	86.1	721.3 ± 57.2	7.93	90.2
1’-OH-Midazolam	75	71.47 ± 3.50	4.90	95.4	74.56 ± 6.18	8.29	99.4
	400	382.3 ± 23.0	6.02	95.6	378.0 ± 14.4	3.80	94.5
	4000	3523 ± 136	3.86	88.1	3661 ± 272	7.42	91.6
Dextromethorphan	75	64.67 ± 10.80	16.7	83.0	66.46 ± 7.47	11.2	87.5
	80	356.0 ± 14.7	4.14	89.0	371.8 ± 19.6	5.27	92.9
	800	3767 ± 186	4.93	94.2	3741 ± 161	4.29	93.6
Dextrophan	15	12.67 ± 2.63	20.7	84.6	12.87 ± 2.14	16.7	85.8
	400	67.90 ± 4.48	6.60	84.9	72.92 ± 5.45	7.48	91.1
	4000	700.0 ± 25.9	3.71	87.5	736.8 ± 39.4	5.35	92.1
Diclofenac	75	86.20 ± 6.77	7.86	115	90.33 ± 21.56	23.9	121
	400	468.3 ± 11.2	2.40	117	421.8 ± 48.6	11.5	106
	4000	3647 ± 123	3.38	91.1	4148 ± 604	14.6	104
4’-OH-Diclofenac	15	15.70 ± 2.48	15.8	105	17.61 ± 3.02	17.2	118
	80	86.87 ± 15.76	18.2	109	81.39 ± 12.65	15.6	102
	800	826.3 ± 20.2	2.45	103	876.6 ± 102.8	11.7	110

Chlorzoxazone	75	87.60	±	8.88	10.1	117	92.79	±	16.50	17.8	124
	400	429.3	±	51.6	12.0	107	413.4	±	52.2	12.6	103
	4000	3716	±	311	8.36	92.9	4290	±	700	16.3	107
6'-OH-Chlorzoxazone	15	16.33	±	4.71	28.8	109	16.64	±	3.60	21.6	111
	80	84.17	±	14.1	16.8	105	81.91	±	34.78	12.8	116
	800	678.3	±	157.8	23.3	84.8	840.1	±	194.5	23.2	105

Table 3. Effects of KTZ and α-NF on pharmacokinetic parameters of individual drugs and metabolites. Data were fit to a non-compartmental PK model. ‡Given incomplete data points because some were below quantification limits, a sparse data model was used. Values represent mean ±SD generated from 6 mice. ***$p < 0.001$, **$p < 0.01$, and *$p < 0.05$ when compared to control (One-way ANOVA with Bonferroni post-hoc tests).

Substrate	Treatment	C_{max}	$AUC_{0\rightarrow\infty}$	% Extrap	$t_{1/2}$ (h)	CL/F (L/h)	V_z/F (L)
MDZ	**Control**	290.8 ± 89.7 nM	347.3 ± 91.2 nM·h	10.00	0.858 ± 0.297	0.282 ± 0.080	0.357 ± 0.160
	KTZ	472.8 ± 214.9 nM	978.2 ± 34.8 nM·h ***	22.17	1.26 ± 0.65	0.108 ± 0.047***	0.178 ± 0.065*
	α-NF	208.7 ± 51.3 nM	258.0 ± 29.7 nM·h	7.12	0.739 ± 0.174	0.361 ± 0.044	0.378 ± 0.070
PHE	**Control**	2.182 ± 0.851 µM	613.7 ± 170.8 nM·h	2.74	0.228 ± 0.055	0.803 ± 0.169	0.259 ± 0.064
	KTZ	0.775 ± 0.666 µM**	207.1 ± 161.5 nM·h	6.31	0.213 ± 0.123	5.03 ± 5.12	1.20 ± 0.91*
	α-NF	2.167 ± 0.445 µM	1.454 ± 0.430 µM·h ***	1.93	0.440 ± 0.190*	0.344 ± 0.087	0.211 ± 0.081
DXM	**Control**	592.8 ± 226.0 nM	1.596 ± 0.490 µM ·h	39.68	1.96 ± 0.45	144 ± 6.2	37.7 ± 8.6
	KTZ	974.0 ± 472.0 nM	4.011 ± 2.324 µM·h *	45.32	2.36 ± 0.46	6.40 ± 4.55	19.8 ± 12.0
	α-NF	381.0 ± 147.7 nM	1.192 ± 0.651 µM ·h	34.13	1.76 ± 0.54	29.7 ± 22.7	62.7 ± 34.2
DIC	**Control**	9.247 ± 3.762 µM	14.68 ± 7.06 µM·h	20.57	1.21 ± 0.37	0.386 ± 0.152	0.634 ± 0.260
	KTZ	20.32 ± 10.45 µM*	52.77 ± 27.62 µM·h **	39.30	1.90 ± 0.43	0.0866 ± 0.106	0.200 ± 0.190
	α-NF	8.218 ± 4.138 µM	9.786 ± 6.136 µM·h	22.13	1.51 ± 0.86	0.553 ± 0.331	1.28 ± 0.59*
CLZ	**Control**	41.91 ± 11.47 µM	45.03 ± 5.35 µM·h	6.73	0.660 ± 0.237	1.12 ± 1.03	0.910 ± 0.651
	KTZ	109.5 ± 58.4 µM *	119.5 ± 50.42 µM·h *	13.2	0.767 ± 0.173	0.218 ± 0.104	0.228 ± 0.112*
	α-NF	71.29 ± 37.52 µM	91.55 ± 30.90 µM·h	7.40	0.688 ± 0.240	0.384 ± 0.216	0.329 ± 0.089

Metabolite	Treatment	C_{max}	$AUC_{0\rightarrow\infty}$	% Extrap	$t_{1/2}$ (h)
1'-OH-MDZ	**Control**	3.758 ± 0.750 µM	10.19 ± 1.89 µM·h	28.73	1.49 ± 0.22
	KTZ	2.992 ± 0.628 µM	17.72 ± 9.03 µM·h	58.95	3.70 ± 1.64**
	α-NF	4.505 ± 0.491 µM	13.27 ± 4.39 µM·h	34.56	1.73 ± 0.53
APAP	**Control**	500.0 ± 69.4 nM	529.6 ± 59.5 nM·h	1.86	0.475 ± 0.097
	KTZ	381.5 ± 186.2 nM	364.4 ± 384.3 nM·h *	2.64	0.537 ± 0.087
	α-NF	362.2 ± 140.7 nM	379.2 ± 80.1 nM·h **	3.11	0.529 ± 0.116
DXO	**Control**	53.6 ± 19.4 nM	87.9 ± 9.4 nM·h	16.40	1.08 ± 0.45
	KTZ	25.3 ± 10.7 nM *	61.5 ± 19.2 nM·h*	30.00	1.34 ± 0.21
	α-NF	40.1 ± 14.3 nM	56.6 ± 18.6 nM·h	20.88	0.948 ± 0.33
4'-OH-DIC	**Control**	141.6 ± 57.5 nM	171.5 ± 56.3 nM·h	14.61	1.09 ± 0.25
	KTZ	36.4 ± 21.3 nM **	97.8 ± 41.3 nM·h *	30.05	1.56 ± 0.17*
	α-NF‡	180.8 nM	8.4 nM·h	3.20	2.10
6-OH-CLZ	**Control**	43.33 ± 4.62 nM	40.7 ± 10.4 nM·h	16.77	0.526 ± 0.083
	KTZ	16.47 ± 4.73 nM ***	51.4 ± 19.2 nM·h	33.02	4.16 ± 1.72**
	α-NF‡	5.043 nM	7.7 nM·h	66.4	1.15

Table 4. Effects of PCN and 3-MC on pharmacokinetic parameters of individual drugs and metabolites. Data were fit to a non-compartmental PK model. ‡Given incomplete data points because some were below quantification limits, a sparse data model was used. Not determined (n.d.) due to insufficient data points representing the elimination phase. Values represent mean ±SD generated from 6 mice. ***$p < 0.001$, **$p < 0.01$, and *$p < 0.05$ when compared to control (One-way ANOVA with Bonferroni post-hoc tests).

Substrate	Treatment	C_{max}	$AUC_{0\rightarrow\infty}$	% Extrap	$t_{1/2}$ (h)	CL/F (L/h)	V_z/F (L)
MDZ	**Control**	173.0 ± 53.7 nM	321.5 ± 51.0 nM·h	21.93	1.36 ± 0.27	0.288 ± 0.051	0.558 ± 0.113
	PCN‡	16.06 ± 13.4 nM***	13.1 ± 3.7 nM·h	1.24	0.52‡	3.8×10^{-5}	1.8×10^{3}
	3-MC	56.90 ± 11.8 nM***	74.6 ± 32.5 nM·h***	13.12	0.867 ± 0.274*	1.26 ± 0.45**	1.51 ± 0.63*
PHE	**Control**	425.8 ± 256.9 nM	154.4 ± 93.3 nM·h	18.37	0.466 ± 0.137	3.74 ± 1.57	2.52 ± 1.47
	PCN	550.0 ± 386.2 nM	150.1 ± 68.4 nM·h	10.64	0.155 ± 0.044**	3.24 ± 1.59	0.761 ± 0.589
	3-MC‡	72.0	4.6 nM·h	0.01	n.d.	n.d.	n.d.
DXM	**Control**	237.2 ± 88.2 nM	646.9 ± 137.6 nM·h	25.44	1.39 ± 0.36	39.6 ± 12.3	122 ± 85
	PCN	143.4 ± 60.6 nM	213.0 ± 36.4 nM·h **	30.84	1.09 ± 0.47	158 ± 57	220 ± 53
	3-MC	154.5 ± 97.9 nM	42.3 ± 82.5 nM·h **	27.14	1.20 ± 0.81	169 ± 121	206 ± 70
DIC	**Control**	49.15 ± 13.99 µM	45.23 ± 14.39 µM·h	1.78	0.418 ± 0.043	1.37 ± 0.97	0.797 ± 0.504
	PCN	6.592 ± 2.613 µM***	7.23 ± 2.81 µM·h ***	12.32	0.979 ± 0.410*	2.05 ± 1.34	2.38 ± 1.17**
	3-MC	29.75 ± 9.12 µM*	17.20 ± 4.8 µM·h ***	9.59	1.03 ± 0.33*	0.616 ± 0.390	0.801 ± 0.290
CLZ	**Control**	199.0 ± 61.9 µM	153.3 ± 43.5 µM·h	0.94	0.380 ± 0.062	1.93 ± 1.22	0.999 ± 0.565
	PCN	23.25 ± 6.91 µM ***	16.6 ± 4.9 µM·h ***	4.09	0.732 ± 0.314	4.02 ± 2.74	3.96 ± 2.02
	3-MC	4.645 ± 1.138 µM ***	3.18 ± 0.91 µM·h ***	7.09	1.04 ± 0.401**	9.06 ± 5.63*	11.6 ± 5.2***

Metabolite	Treatment	C_{max}	$AUC_{0\rightarrow\infty}$	% Extrap	$t_{1/2}$ (h)
1'-OH-MDZ	**Control**	4.540 ± 0.449 µM	11.88 ± 9.56 µM·h	32.67	1.48 ± 0.88
	PCN	1.950 ± 0.528 µM***	1.81 ± 0.38 µM·h*	6.66	0.672 ± 0.276
	3-MC	3.532 ± 0.616 µM*	7.46 ± 1.69 µM·h	22.81	1.29 ± 0.43
APAP	**Control**	523.6 ± 190.8 nM	671.6 ± 237.6 nM·h	8.59	0.820 ± 0.233
	PCN	623.3 ± 140.5 nM	367.8 ± 70.7 nM·h*	1.85	0.467 ± 0.172*
	3-MC	336.8 ± 139.0 nM	225.8 ± 62.7 nM·h**	3.81	0.702 ± 0.227
DXO	**Control**	29.9 ± 14.8 nM	56.3 ± 10.3 nM·h	15.56	1.17 ± 0.38
	PCN	15.8 ± 6.3 nM	26.1 ± 8.7 nM·h**	52.30	1.16 ± 0.43
	3-MC	14.6 ± 9.6 nM	20.8 ± 46.5 nM·h**	18.66	0.376 ± 0.181
4'-OH-DIC	**Control**	240.2 ± 90.0 nM	631.1 ± 250.2 nM·h	32.76	1.85 ± 0.34
	PCN	747.5 ± 435.2 nM*	315.6 ± 133.9 nM·h*	14.77	1.28 ± 0.49
	3-MC	173.3 ± 61.0 nM	362.4 ± 151.7 nM·h	43.10	2.56 ± 1.19
6-OH-CLZ	**Control**	60.7 ± 51.8 nM	31.9 ± 12.8 nM·h	12.24	0.422 ± 0.135
	PCN‡	458.4 ± 134.1 nM***	171.1 nM·h***	0.01	0.357‡
	3-MC	33.7 ± 10.9 nM	21.6 ± 2.8 nM·h	37.70	0.620 ± 0.049

Table 5. Effects of miR-34a on the pharmacokinetic parameters of individual drugs and metabolites. Data were fit to a non-compartmental PK model. Values represent mean ±SD generated from 6 mice. $p < 0.001$, $^{**}p < 0.01$, and $^{*}p < 0.05$ when compared to control (One-way ANOVA with paired Bonferroni post-hoc tests).

Substrate	Treatment	C_{max}	$AUC_{0\rightarrow\infty}$	% Extrap	$t_{1/2}$ (h)	CL/F (L/h)	V_z/F (L)
MDZ	**Control**	15.9 ± 8.9 nM	23.4 ± 7.5 nM·h	20.54	1.237 ± 0.710	6.995 ± 4.317	3.822 ± 1.115
	miR-34a	20.7 ± 3.0 nM	37.4 ± 5.4 nM·h ***	17.72	1.182 ± 0.245	4.122 ± 0.897	2.432 ± 0.351
PHE	**Control**	229.0 ± 68.2 nM	74.3 ± 14.6 nM·h	13.27	0.256 ± 0.068	2.349 ± 0.981	6.243 ± 1.295
	miR-34a	225.7 ± 96.8 nM	91.3 ± 13.8 nM·h **	14.95	0.297 ± 0.044	2.166 ± 0.461	5.032 ± 0.708
DXM	**Control**	247.6 ± 88.1 nM	906.6 ± 388.7 nM·h	37.30	3.052 ± 2.771	70.33 ± 20.04	23.56 ± 14.11
	miR-34a	349.2 ± 74.8 nM ***	1276 ± 296 nM·h *	49.15	2.762 ± 0.984	50.63 ± 11.41	13.81 ± 4.80
DIC	**Control**	841.0 ± 174.5 nM	2.345 ± 1.768 µM·h	30.09	1.832 ± 1.588	7.630 ± 5.150	5.067 ± 4.019
	miR-34a	1.448 ± 0.239 µM ***	2.612 ± 0.752 µM·h	25.69	1.558 ± 0.480	4.054 ± 1.725	2.026 ± 1.058
CLZ	**Control**	9.856 ± 2.443 µM	8.722 ± 1.248 µM·h	4.16	0.644 ± 0.158	6.751 ± 3.613	8.152 ± 6.015
	miR-34a	10.73 ± 1.866 µM	11.14 ± 1.80 µM·h *	5.56	0.659 ± 0.153	4.328 ± 2.053	5.089 ± 3.450

Metabolite	Treatment	C_{max}	$AUC_{0\rightarrow\infty}$	% Extrap	$t_{1/2}$ (h)
1'-OH-MDZ	**Control**	2.665 ± 0.566 µM	7.807 ± 3.186 µM·h	29.44	1.432 ± 0.553
	miR-34a	2.443 ± 0.377 µM	7.424 ± 1.275 µM·h	32.67	1.630 ± 0.249
APAP	**Control**	2.147 ± 0.395 µM	1.797 ± 0.336 µM·h	5.08	0.763 ± 0.265
	miR-34a	1.700 ± 0.169** µM	1.640 ± 0.158 µM·h	4.86	0.692 ± 0.154
DXO	**Control**	175.6 ± 48.8 nM	307.9 ± 41.7 nM·h	22.18	1.271 ± 0.160
	miR-34a	163.2 ± 16.7 nM	358.9 ± 51.8 nM·h	25.66	1.417 ± 0.144
4'-OH-DIC	**Control**	136.5 ± 51.4 nM	275.6 ± 105.8 nM·h	20.94	1.286 ± 0.372
	miR-34a	126.0 ± 48.9 nM	284.5 ± 127.1 nM·h	33.77	1.984 ± 0.656
6-OH-CLZ	**Control**	45.57 ± 0.02 nM	42.2 ± 11.6 nM·h	25.77	0.629 ± 0.352
	miR-34a	47.50 ± 0.01 nM	40.0 ± 5.5 nM·h	17.75	0.684 ± 0.150

Table 6. Effects of miR-34a on *in vitro* intrinsic clearance of CYP probe substrates. DXM intrinsic clearance was marginally attenuated in liver microsomes derived from mice treated with miR-34a agent, as compared to the control. Data were fit to a mono-exponential decay model (or biphasic decay for MDZ) to derive $t_{1/2}$ and CL_{int}. Data represent mean ± SD (N = 5 per group). DIC and CLZ data are not fit to any model because there was minimal substrate depletion.

Substrate	Treatment	$t_{1/2}$ (min)	CL_{int} (ml/min/mg protein)
MDZ	**Control**	2.52 ± 0.26	0.20 ± 0.04
	miR-34a	2.60 ± 0.34	0.24 ± 0.08
PHE	**Control**	14.62 ± 6.27	0.09 ± 0.02
	miR-34a	12.56 ± 2.19	0.11 ± 0.01
DXM	**Control**	14.34 ± 2.55	0.10 ± 0.01
	miR-34a	18.49 ± 1.38 **	0.07 ± 0.01 **

Table 7. Comparison of the degrees of interactions between several paired drugs in various species using different dosing regimens. p.o., oral gavage/administration; i.p., intraperitoneal injection; i.v., intravenous injection; i.g., intragastric administration; i.d., intraduodenal injection.

Substrate	Inhibitor	Change of AUC	Dosing regimen	Species	Reference
MDZ	KTZ	16-fold increase	3 doses of 200 mg KTZ every 12 h, p.o.; 90 min after last dose of KTZ, 6 mg MDZ plus 200 mg KTZ, p.o.	Humans	(Tsunoda et al., 1999)
	KTZ	7.7-fold increase	200 mg KTZ for 12 days, p.o.; 1 h after the last dose of KTZ, 10 mg MDZ, p.o.	Humans	(Lam et al., 2003)
	KTZ	5.0-fold increase	200 mg KTZ, p.o.; 2 h later, 2 mg MDZ, p.o.	Humans	(McCrea et al., 1999)
	KTZ	6.5-fold increase	10 mg/kg KTZ, i.p.; 30 min later, 15 mg/kg MDZ, i.g.; 180 min later, 5 mg/kg KTZ, i.p., to maintain serum KTZ concentrations at 2 μg/ml or higher	Sprague-Dawley rats	(Kotegawa et al., 2002)
	KTZ	1.5-fold increase	10 mg/kg KTZ, i.p.; 30 min later, 5 mg/kg MDZ, i.v.; 180 min later, 5 mg/kg KTZ, i.p., to maintain serum KTZ concentrations at 2 μg/ml or higher	Sprague-Dawley rats	(Kotegawa et al., 2002)
	KTZ	3.3-fold increase	40 mg/kg KTZ, p.o.; 45 min later, 2.5 mg/kg MDZ, p.o.	FVB/N mice	(Granvil et al., 2003)
	KTZ	6.3-fold increase	40 mg/kg KTZ, p.o.; 45 min later, 2.5 mg/kg MDZ, p.o.	CYP3A4-humanized FVB/N mice	(Granvil et al., 2003)
	KTZ	2.8-fold increase	50 mg/kg KTZ, i.p.; 1 h later, 1 mg/kg MDZ in a cocktail, p.o.	CD-1 mice	Current study
	PCN	10% increase	10 mg/kg PCN for 3 days, i.g.; 0.3 mg/kg MDZ, i.v.	C57BL/6J mice	(Pang et al., 2011)
	PCN	25-fold decrease	40 mg/kg PCN for 3 days, i.p.; 1 mg/kg MDZ in a cocktail, p.o.	CD-1 mice	Current study

PHE	α-NF	1.8-fold increase	7 mg/kg α-NF, i.v.; 15 min later, 5 mg/kg PHE, i.v.	Sprague-Dawley rats	(Zhuang et al., 2013)
	α-NF	2.3-fold increase	100 mg/kg α-NF, i.p.; 1 h later 2.8 mg/kg PHE in a cocktail, p.o.	CD-1 mice	Current study
	3-MC	4.9-fold decrease	20 mg/kg 3-MC for 2 days, p.o.; 20 mg/kg PHE, i.v.	Wistar rats	(Klippert et al., 1983)
	3-MC	13-fold decrease	20 mg/kg 3-MC for 2 days, p.o.; 20 mg/kg PHE, i.d.	Wistar rats	(Klippert et al., 1983)
	3-MC	33-fold decrease	50 mg/kg 3-MC for 3 days, i.p.; 2.8 mg/kg PHE in a cocktail, p.o.	CD-1 mice	Current study

DMD Fast Forward. Published on March 2, 2017 as DOI: 10.1124/dmd.116.074344
This article has not been copyedited and formatted. The final version may differ from this version.

Figure 1

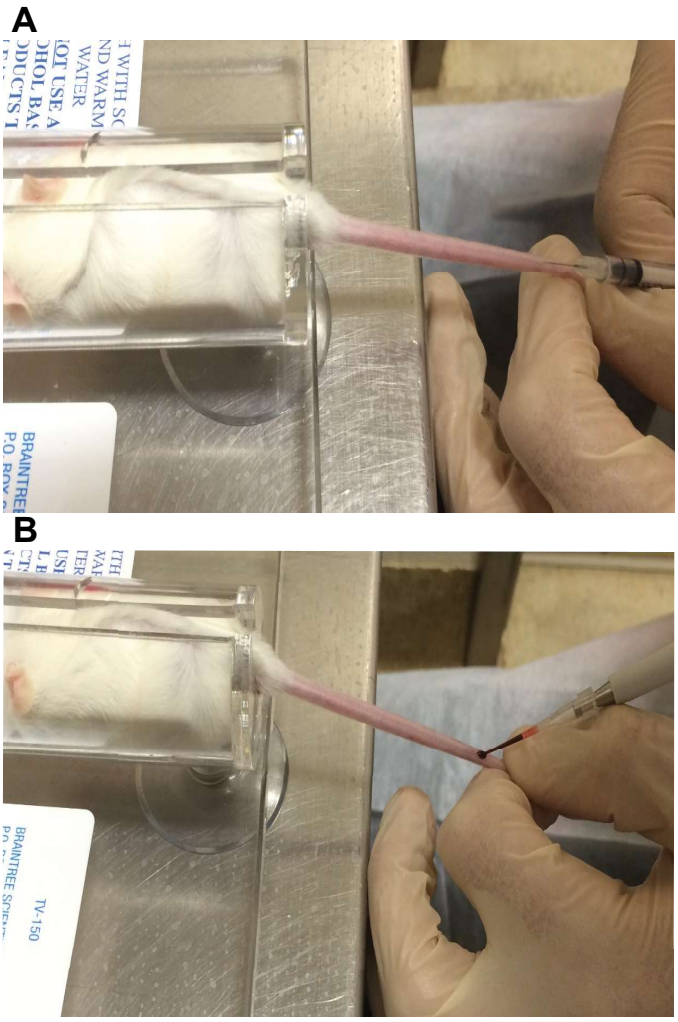

DMD Fast Forward. Published on March 2, 2017 as DOI: 10.1124/dmd.116.074344
This article has not been copyedited and formatted. The final version may differ from this version.

Figure 2

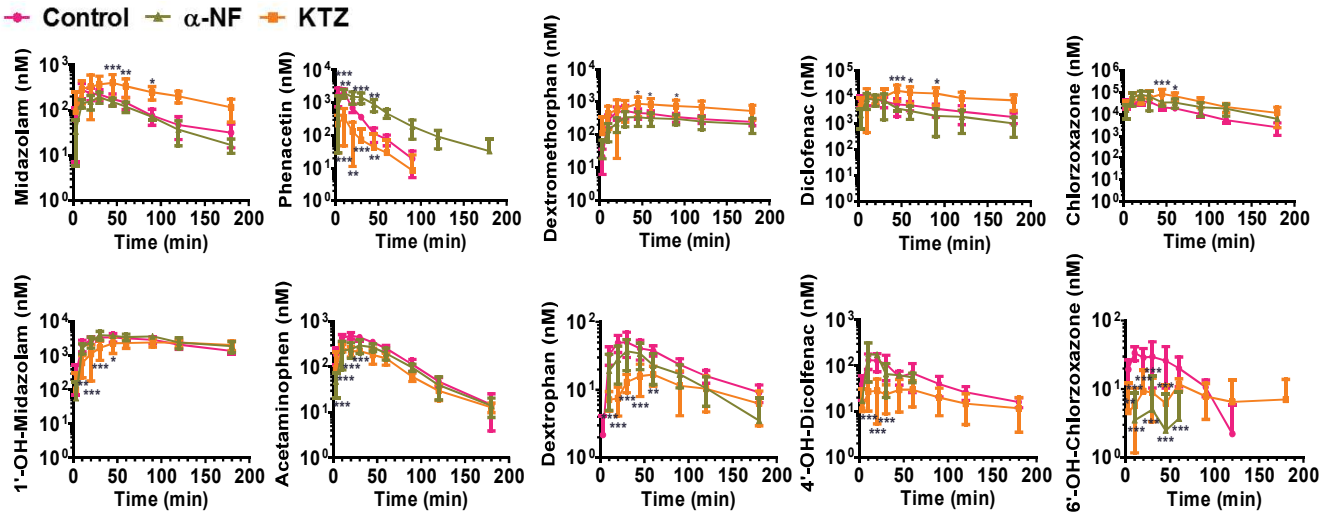

DMD Fast Forward. Published on March 2, 2017 as DOI: 10.1124/dmd.116.074344
This article has not been copyedited and formatted. The final version may differ from this version.

Figure 3

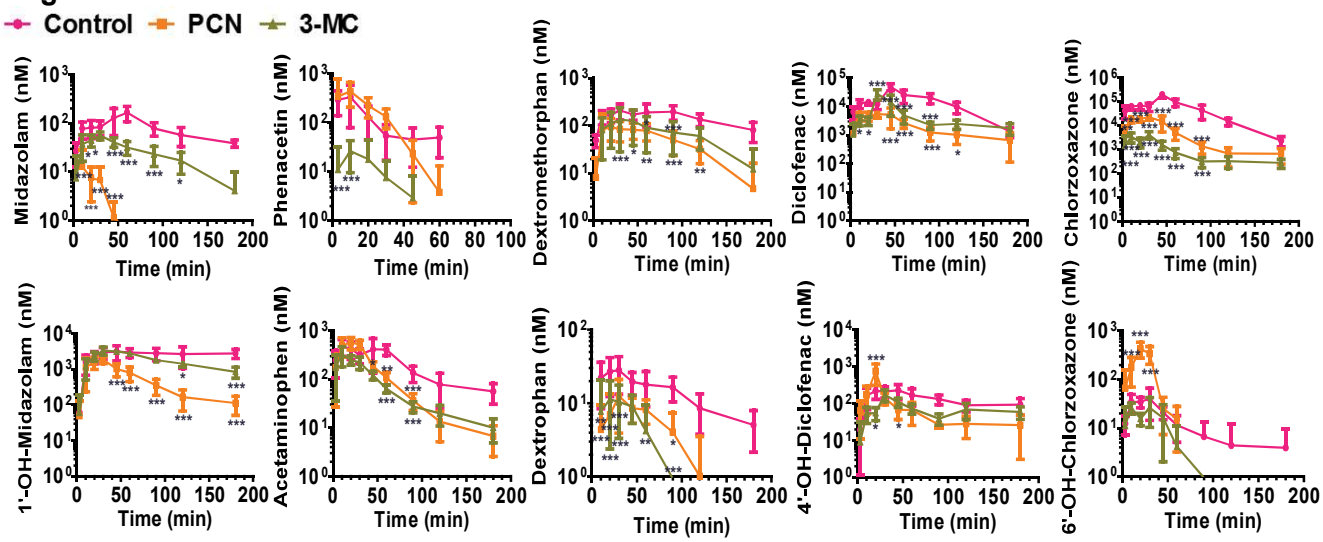

DMD Fast Forward. Published on March 2, 2017 as DOI: 10.1124/dmd.116.074344
This article has not been copyedited and formatted. The final version may differ from this version.

Figure 4

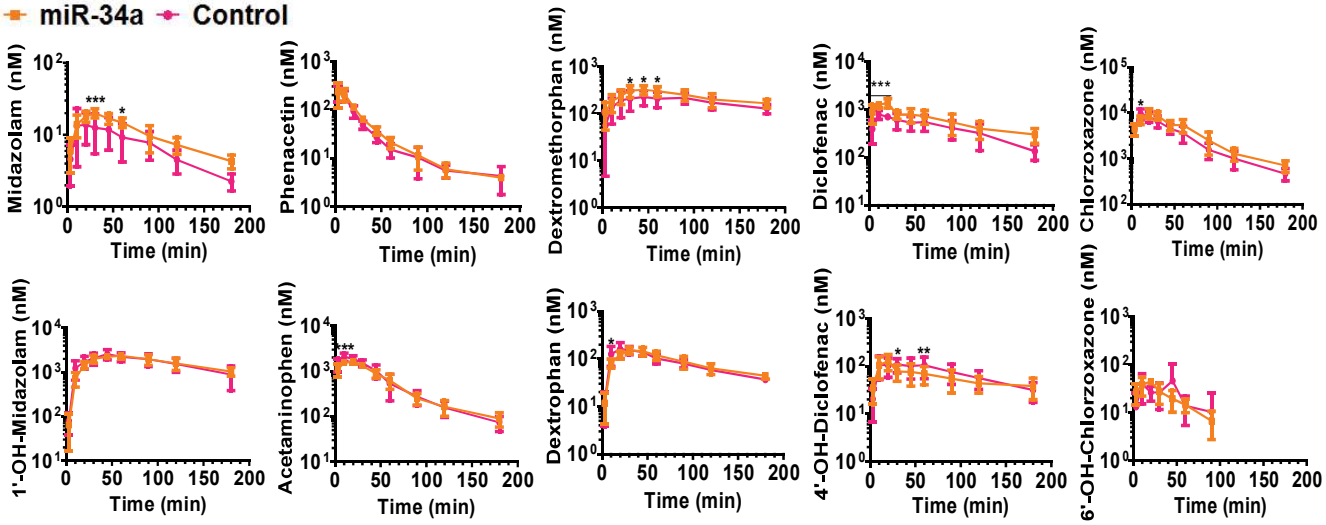

DMD Fast Forward. Published on March 2, 2017 as DOI: 10.1124/dmd.116.074344
This article has not been copyedited and formatted. The final version may differ from this version.

Figure 5